Available online at www.sciencedirect.com
SCIENCE DIRECT®
Journal of Power Sources 145 (2005) 40–49
JOURNAL OF POWER SOURCES
www.elsevier.com/locate/jpowsour

Conceptual design of the integration of the reforming process in high temperature fuel cells

Peter Heidebrecht [a], Kai Sundmacher [a, b, *]

[a] *Otto-von-Guericke-University Magdeburg, Process Systems Engineering, Universitätsplatz 2, D-39106 Magdeburg, Germany*
[b] *Max-Planck-Institute for Dynamics of Complex Technical Systems, Sandtorstraße 1, D-39106 Magdeburg, Germany*

Received 12 May 2004; received in revised form 15 December 2004; accepted 31 December 2004
Available online 23 February 2005

Abstract

The integration of the endothermic reforming reactions and the exothermic electrochemical reactions in a molten carbonate fuel cell (MCFC) is investigated with a mathematical steady state anode model. The dimensionless model consists of only a few equations based on the description of physical phenomena, and is thus easily solved and interpreted. The equations and their derivation are presented and three different applications of the model are demonstrated. It proves to be a useful tool for an intuitive understanding of the interactions of reforming and electrochemical processes, but it can also yield quantitative results for flow sheet design of MCFC with internal reforming.

Keywords: Steam reforming; Process integration; Mathematical modelling; MCFC

1. Introduction

The storage and preparation of fuels for fuel cells is currently under investigation by numerous research and development groups worldwide. Its impact on the electric efficiency and profitability of any type of fuel cell system probably is as important as the fuel cell design itself. Among the many proposed and investigated variants to provide hydrogen for the electrochemical process, the steam reforming concept has emerged as one of the most promising. Fuels, which can either be stored easily or which is otherwise available at the fuel cell site, for example gasoline, diesel fuel or natural gas, undergoes a reaction which produces hydrogen and several by-products. Often times this reforming product has to be cleaned up before being fed into the fuel cell.

The key issue with reforming is the supply of heat to the endothermic process and the demand for high temperatures in order to obtain high reaction rates and favourable chemical equilibria. While for low temperature fuel cells this heat has to be provided by external sources, for example the direct oxidation of a part of the feed gas, high temperature fuel cells like the SOFC and the MCFC directly provide the heat required for the reforming process. This leads to the internal reforming concept, in which the endothermic reforming process is integrated into the fuel cell, where the exothermic electrochemical reactions occur. The interactions of both processes are based on their substantial and energetical coupling and their effects are manifold. The use of mathematical models is probably the best way to gain deeper understanding of these coherences.

Some authors working on the modelling of MCFC include the reforming reactions in their equations in different ways. He and Chen [1] and Yoshiba et al. [2] only consider the water–gas shift reaction in their spacially distributed anode channel. Due to its high rate they assume it to be in thermodynamic equilibrium. Lukas et al. [3] and Park et al. [4] also describe the water–gas shift reaction as being in equilibrium, but they additionally include the steam reforming reaction of methane as an irreversible reaction with a finite reaction rate expression. Especially, Park focuses on the effect of an

* Corresponding author. Tel.: +49 391 6110350; fax: +49 391 6110353.
E-mail address: sundmacher@mpi-magdeburg.mpg.de (K. Sundmacher).

0378-7753/$ – see front matter © 2005 Elsevier B.V. All rights reserved.
doi:10.1016/j.jpowsour.2004.12.037

Nomenclature

Latin symbols

Arr_j	Arrhenius number of reaction j
Da_j	Damköhler number of reaction j
F	stoichiometric factor
k_j	Arrhenius term of reaction j
K_j	equilibrium constant of reaction j
r_j	reaction rate of reaction j
P_{el}	electric power
R	anode gas recycle ratio
U_{cell}	cell voltage

Greek symbols

γ	molar flow density in channel
Γ	molar flow
$\tilde{\Gamma}$	corrected molar flow
ζ	spacial parameter
ϑ	temperature
λ_{air}	air number
$\nu_{i,j}$	stoichiometric coefficient of component i in reaction j
$\bar{\nu}_j$	sum of stoichiometric coefficients of reaction j
ξ_j	extent of reaction j
$\xi_{j,\max}$	normalisation factor for ξ_j
ϕ_{E}	electric potential in electrolyte
$\Delta\phi_{j,0}$	standard equilibrium potential difference of reaction j
χ_i	molar fraction of component i

Subscripts

ref	reforming reaction
ox	oxidation reaction
red	reduction reaction
i	general component index
feed	system feed
j	general reaction index
max	see above $\xi_{j,\max}$
0	standard condition
in	channel inlet
back	anode gas recycle
out	channel outlet
ex	exhaust, catalytic burner feed
c	cathode
air	burner air

Superscripts

+	forward reaction direction
−	backward reaction direction
0	equilibrium

indirect reforming unit in the stack. Although all of these models consider the influence of non-electrochemical reactions inside the fuel cell, none of them is suitable to easily and intuitively explain their impact on the system. This is mostly due to the general complexity of these detailed models.

Other authors discuss suitable system design for high temperature fuel cells with internal reforming. Fellows [5] and Kortbeek and ottervanger [6] propose complex configurations, including gas recycling, side feeding and cell cascades. The effects of these measures can be simulated by sophisticated models, but these do not offer an intuitive understanding of the interaction of reforming and electrochemical reactions nor a quick and simple tool for conceptual system design.

Therefore, a model is required that describes the basics of a high temperature fuel cell in a physically meaningful way and fulfils these requirement. In addition, an easily interpretable diagram is useful for the illustration of the numerical results. The objective of this paper is to develop such a tool on the example of a methane-fed MCFC, and to demonstrate its usefulness for several applications.

2. Technical background

The working principle of the Molten Carbonate Fuel Cell is illustrated in Fig. 1. The anode is fed with a preheated mixture of desulphurised natural gas and steam at a steam to carbon ratio of about S/C = 2.5. This feed gas is converted via steam reforming into a hydrogen rich gas mixture at the reformer catalyst, which is placed inside the anode channel. Carbon monoxide is a major by-product of this reforming process. Simultaneously, the water gas shift reaction transforms carbon monoxide into carbon dioxide and additional hydrogen:

$$\mathrm{CH_4 + H_2O \leftrightarrow CO + 3H_2} \quad (1)$$

$$\mathrm{CO + H_2O \leftrightarrow CO_2 + H_2} \quad (2)$$

The equilibrium limitations of these two reforming reactions are overcome by continuous removal of hydrogen and carbon monoxide, which is directly oxidised electrochemically at the anodic electrode. There, these substances react with carbonate ions from the electrolyte producing carbon

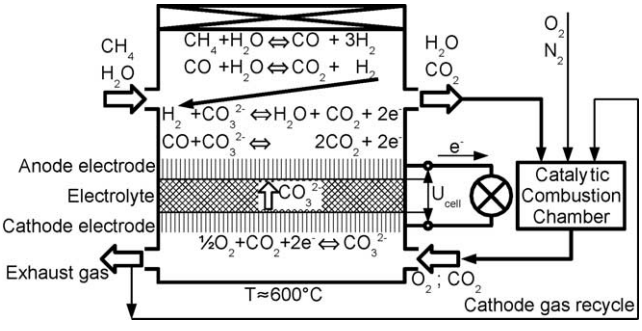

Fig. 1. Working principle of the MCFC with direct internal reforming.

dioxide, water and electrons according to the following stoichiometric relations:

$$H_2 + CO_3^{2-} \leftrightarrow H_2O + CO_2 + 2e^- \quad (3)$$

$$CO + CO_3^{2-} \leftrightarrow 2CO_2 + 2e^- \quad (4)$$

In addition to the mass coupling, the reforming process, which is overall endothermic, is energetically coupled to the exothermic oxidation reactions, thus the heat required for the generation of hydrogen is provided.

The anode exhaust gas is mixed with air and the unoxidised components are fully oxidised in a catalytic combustion chamber. Because air is fed in excess the exhaust gas from the burner still contains a significant amount of oxygen. This gas is then fed to the cathode channel where the electrochemical reduction takes place. New carbonate ions are produced from carbon dioxide and oxygen according to the backward direction of the following cathode reaction:

$$CO_3^{2-} \leftrightarrow \tfrac{1}{2}O_2 + CO_2 + 2e^- \quad (5)$$

The carbonate ions are transported towards the anode electrode through the electrolyte, which is a eutectic carbonate melt. Often times, a part of the cathodic exhaust gas is recycled back towards the catalytic combustion chamber and the remaining gas leaves the fuel cell. Due to its high temperature of about 600 °C, the exhaust gas can be used for subsequent steam generation, for additional production of electric energy via a micro turbine or for other purposes.

Besides the possibility to form hydrogen inside the anode channel, it can also be produced otherwise. Fig. 2 shows the three basic reforming concepts for high temperature fuel cells. The external reforming (ER) happens in a separate vessel outside the cell stack. Any arbitrary temperature can be applied, but high temperatures require external heating. For temperatures well below the cell temperature, the cell exhaust gas can be used to supply the required reaction heat to the ER. The main advantage of the ER is that its design and operating conditions are largely independent from those of the fuel cell.

The indirect internal reformer (IIR) is situated in the cell stack in special reforming channels, where only reforming reaction takes place. This concept features energetic coupling with the exothermic oxidation process. The main advantage is that no external heat exchanger is required, as the separator plate between IIR and anode channel adopts this function.

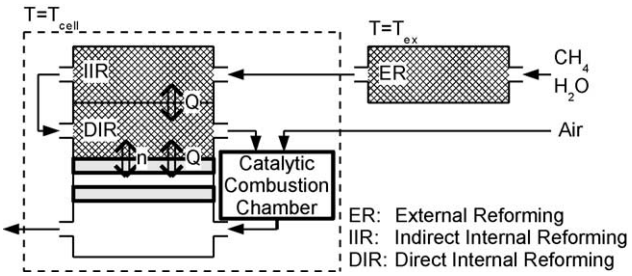

Fig. 2. Reforming concepts for high temperature fuel cells.

The IIR can be seen as an external reformer operating at fuel cell temperature.

Finally, the substantial and energetic coupling of the reforming and electrochemical processes leads to the direct internal reforming (DIR) concept. Not only is heat exchanged between both, but also the products of the reforming process are continuously removed by the oxidation reactions. This is a highly integrated concept, which offers the chance for high system efficiency, but it requires sophisticated system design in order to work properly.

3. Modelling

With the numerous possible combinations of different reforming concepts and due to the various flow sheet options like gas recycling, cell cascading and side feeding, a tool is required for the analysis of these configurations. This tool should be

- physically meaningful in order to allow for an intuitive understanding of its results,
- flexible, so that one can also analyse additional aspects besides those mentioned here,
- fast to solve, as the task here is not a detailed and exact prediction of states, but should rather yield principal insight and show up tendencies,
- easily illustrated and interpretable.

In this section, a mathematical model called the steady state anode model is introduced which fulfils these requirements. First, the complete model equations are given and their derivation is briefly indicated. In the second part an accompanying diagram to this model is introduced, in which the simulation results can be displayed.

3.1. Model derivation

The steady state anode model is derived from a fully dynamic, spacially two-dimensional description of a single cross-flow MCFC [7,8]. As thar model is completely formulated in terms of dimensionless variables, the steady state anode model is dimensionless as well. It is derived under the following assumptions:

- The system is at steady state.
- Assume a sufficiently high cathode gas recycle ratio, so that the composition and temperature of the cathode gas are approximately constant along the channel.
- As a consequence of the constant cathode gas temperature, the cell temperature is also constant along the spacial coordinate. This temperature is not calculated by an energy balance, but it is given as a parameter. Nevertheless, temperature effects on the reaction rates and the equilibrium constants are considered.
- The cell is operated under ambient pressure conditions. Pressure drop is neglected, as we mainly focus on the substantial interplay of reforming and oxidation.

- The oxidation reaction of carbon monoxide (Eq. (3)) in MCFC is known to be of minor importance compared to the oxidation of hydrogen and is thus neglected.
- Due to the very fast water–gas shift reaction and because the equilibrium of this reaction at high temperatures is on the right hand side of Eq. (2), the amount of carbon monoxide in the anode gas is negligible. Thus, both reforming reactions are condensed into one single reforming reaction:

$$CH_4 + 2H_2O \leftrightarrow CO_2 + 4H_2 \tag{6}$$

- Mass transport in the electrode pores is neglected.
- Instead of galvanostatic cell operation, potentiostatic operating mode is applied. Thus, the cell voltage is given as an operating parameter.
- The ion conduction resistance in the electrolyte perpendicular to the cell plain is negligible. Nevertheless, no ion conduction occurs along the cell plain. Thus the electrolyte has identical electric potentials at the anode and cathode electrode, but these are locally distributed.
- The possibility of anode gas recycling shall be considered.

The resulting equations, i.e. mainly the partial and the total mass balances in the anode channels, are given in dimensionless form in Appendix A. The five ordinary differential equations (ODEs) describe five unknowns in one single anode channel, namely the molar fractions of CH_4, H_2O, H_2 and CO_2 as well as the molar flow density, γ. The cathode gas composition is calculated independently from the ODEs according to a full combustion calculation of the feed stream with air in several algebraic equations (see Appendix A).

To reduce the number of ODEs even further, a physically motivated transformation is applied. The idea is that for a given composition of the feed gas (CH_4/H_2O-mixture, characterised by the steam/carbon-ratio) the composition of the gas at any point in the anode channel or in any of the reforming units is described by only two states: the extent of the reforming reaction, assigned ξ_{ref}, and the extent of the oxidation reaction, assigned ξ_{ox}. These variables are made dimensionless and normalised to unity, so they can be interpreted as follows:

$\xi_{ref} = 0 \Leftrightarrow$ gas is not reformed ...

$\xi_{ref} = 1 \Leftrightarrow$ gas is completely reformed

$\xi_{ox} = 0 \Leftrightarrow$ gas is not oxidised ...

$\xi_{ox} = 1 \Leftrightarrow$ gas is completely oxidised

note that the extent of oxidation reaction is identical to the well known fuel utilisation, relating the rate of electrochemical fuel consumption to the fuel feed rate. Usually, a high fuel utilisation is desirable.

$\xi_{ox} \hat{=}$ fuel utilisation

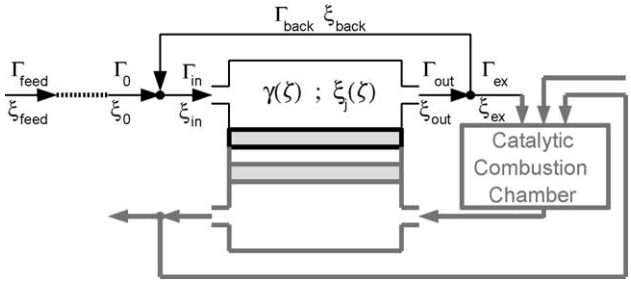

Fig. 3. Flow scheme and assigned variables of the steady state anode model.

with this, the molar fraction of any component can be described as a function of the extents of reaction:

$$\chi_i = \frac{\chi_{i,\text{feed}} + \sum_{j=\text{ref,ox}} \nu_{i,j} \times \xi_j \xi_{j,\max}}{1 + \sum_{j=\text{ref,ox}} \bar{\nu}_j \times \xi_j \xi_{j,\max}} \tag{7}$$

where

$$\chi_{CH_4,\text{feed}} = \frac{1}{1 + S/C}$$

$$\chi_{H_2O,\text{feed}} = \frac{S/C}{1 + S/C}$$

$$\xi_{\text{ref},\max} = \frac{1}{1 + S/C}$$

$$\xi_{\text{ox},\max} = \frac{4}{1 + S/C}$$

In addition to this, the possibility of anode gas recycling shall be considered. Fig. 3 shows the assignments of all molar gas flows inside and outside the anode channel. At steady state, the flows differ due to two reasons: firstly the addition of the recycle flow to the anode inlet, and secondly due to the change of total mole numbers with reactions.

To eliminate the influence of the second mentioned, a corrected molar flow is introduced, marked with a tilde sign. In general, it holds that

$$\Gamma = \tilde{\Gamma} \times \left(1 + \sum_{j=\text{ref,ox}} \bar{\nu}_j \times \xi_j \xi_{j,\max}\right) \tag{8}$$

with this definition, the mixing rules can be set up. They follow from the total and the partial molar balance at the mixing point before the channel inlet (Fig. 3) together with Eqs. (7) and (8). The flows are added, while the mixing gas composition is a linear combination of the gas compositions of both mixed flows according to the law of the lever:

$$\tilde{\Gamma}_{\text{in}} = \tilde{\Gamma}_0 + \tilde{\Gamma}_{\text{back}} \tag{9}$$

$$\xi_{j,\text{in}} = \frac{\tilde{\Gamma}_0 \xi_{j,0} + \tilde{\Gamma}_{\text{back}} \xi_{j,\text{back}}}{\tilde{\Gamma}_0 + \tilde{\Gamma}_{\text{back}}} \tag{10}$$

The extents of reaction inside the channel are described by ordinary differential equations resulting from the continuous

total and partial molar balances. Their derivation is given in Appendix A. The result reads:

$$\frac{\mathrm{d}\xi_j}{\mathrm{d}\zeta} = \frac{\mathrm{Da}_j r_j}{\tilde{\Gamma}_{\mathrm{in}}} \times \frac{1}{\xi_{j,\max}} \tag{11}$$

with

$$j = \mathrm{ref},\ \mathrm{ox}$$

The boundary condition is given at the inlet

$$\xi_j(\zeta = 0) = \xi_{j,\mathrm{in}} \tag{12}$$

The Damköhler numbers for the reforming and the oxidation reaction cannot only be used to adjust finite reaction rate constants of both reactions in the simulation, but each of these reactions can be eliminated by setting the specific Damköhler number to zero. Thus it is possible to simulate a pure reforming channel ($\mathrm{Da}_{\mathrm{ox}} = 0$) or an anode channel without direct internal reforming ($\mathrm{Da}_{\mathrm{red}} = 0$).

In addition to the two ODEs, the reaction kinetics are required. The kinetic expressions are given here in short form. For a full version of these equations we refer the reader to Appendix A. The reforming reaction rate depends on the gas composition and the given temperature parameter, the equilibrium constant is only temperature dependent:

$$r_{\mathrm{ref}}(\xi, \vartheta) = k_{\mathrm{ref}}(\vartheta) \times \left\{ r^{+}_{\mathrm{ref}}(\xi) - \frac{r^{-}_{\mathrm{ref}}(\xi)}{K_{\mathrm{eq,ref}}(\vartheta)} \right\} \tag{13}$$

The oxidation rate depends not only on the gas composition and the temperature parameter, but also on the electric potential difference at the charged double layer of the anode electrode, $\Delta\phi_{\mathrm{a}}$. On the other hand, the reduction reaction rate depends on the electric potential difference at the cathode electrode, $\Delta\phi_{\mathrm{a}}$. Applying a Butler-Volmer type reaction kinetics, we receive:

$$r_{\mathrm{ox}}(\xi, \vartheta, \Delta\phi_{\mathrm{a}}) = k_{\mathrm{ox}}(\vartheta, \Delta\phi_{\mathrm{a}}) \times \left\{ r^{+}_{\mathrm{ox}}(\xi) - \frac{r^{-}_{\mathrm{ox}}(\xi)}{K_{\mathrm{eq,ox}}(\vartheta, \Delta\phi_{\mathrm{a}})} \right\} \tag{14}$$

$$r_{\mathrm{red}}(\xi, \vartheta, \Delta\phi_{\mathrm{c}}) = k_{\mathrm{ox}}(\vartheta, \Delta\phi_{\mathrm{c}}) \times \left\{ r^{+}_{\mathrm{red}}(\xi) - \frac{r^{-}_{\mathrm{red}}(\xi)}{K_{\mathrm{eq,red}}(\vartheta, \Delta\phi_{\mathrm{c}})} \right\} \tag{15}$$

With the Eqs. (14) and (15) containing four unknowns, namely r_{ox}, r_{red}, $\Delta\phi_{\mathrm{a}}$ and $\Delta\phi_{\mathrm{c}}$, two more equations are needed to solve the equations. One of them is the steady state charge balance stating that the current density produced at the anode electrode must be equal to the current density produced at the cathode electrode at any given point in the channel:

$$\mathrm{Da}_{\mathrm{ox}} \times r_{\mathrm{ox}} = \mathrm{Da}_{\mathrm{red}} \times (-r_{\mathrm{red}}) \tag{16}$$

The second equation sums the potential differences at both electrodes, which results in the given cell voltage:

$$\Delta\phi_{\mathrm{a}} + (-\Delta\phi_{\mathrm{c}}) = U_{\mathrm{cell}} \tag{17}$$

Eqs. (14)–(17) contain four unknowns: the anodic and cathodic reaction rates, r_{ox} and r_{ox}, respectively, and the electric potentials at both electrodes, $\Delta\phi_{\mathrm{a}}$ and $\Delta\phi_{\mathrm{c}}$. They have to be solved for the oxidation reaction rate, r_{ox}, which is required in Eq. (11).

As a measure for the system efficiency, the electric power output of a cell is calculated according to

$$P_{\mathrm{el}} = \frac{\Delta\xi_{\mathrm{ox}} U_{\mathrm{cell}}}{F} \tag{18}$$

where

$$\Delta\xi_{\mathrm{ox}} = \xi_{\mathrm{ox}}(\zeta = \zeta_{\mathrm{end}}) - \xi_{\mathrm{ox}}(\zeta = 0) \tag{19}$$

With this, the complete model is described. Outside any channels, Eqs. (9) and (10) describe mixing rules. These might be necessary to calculate the boundary condition (Eq. (12)) for Eq. (11), which together with the reaction rate expressions in Eqs. (13)–(17) describe the state inside such channels.

3.2. The conversion diagram

With only two locally distributed states in the model, it is possible to illustrate any of its results in a phase diagram. In this kind of plot, the independent spacial variable is eliminated by plotting one state versus the other. Fig. 4 shows the extent of the reforming reaction on the horizontal axis and the extent of oxidation reaction on the vertical axis. Because the molar fraction of any component cannot become negative, certain limitations for physically reasonable states in the conversion diagram follow. The extents of reaction may only be situated within the triangle in Fig. 4.

Also indicated in this figure is the fact that for a given temperature and cell voltage, the reaction rates at every point within the allowable region are defined. A positive reforming

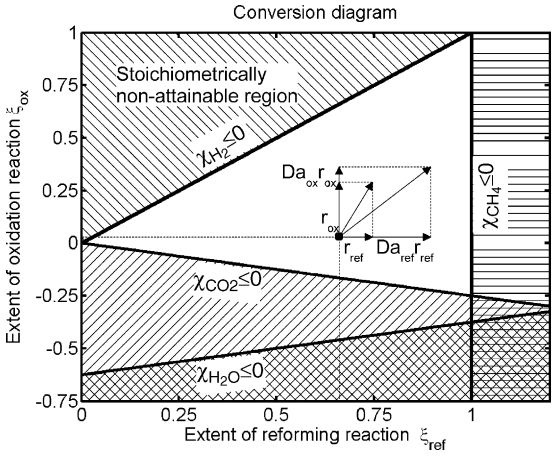

Fig. 4. The conversion diagram, stoichiometrically attainable region and reaction rate vector.

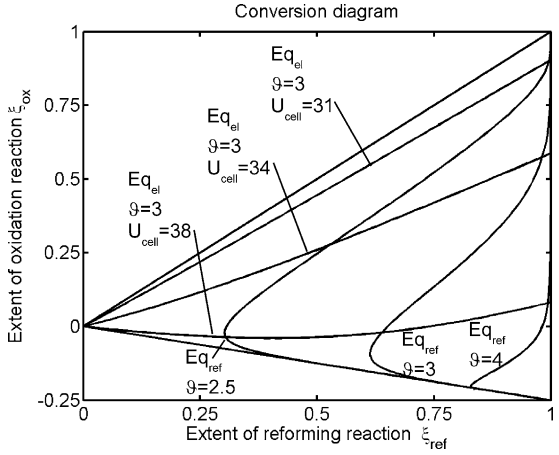

Fig. 5. Reforming equilibrium lines at various temperatures and oxidation equilibrium lines at constant temperature and various cell voltage. The dimensionless numbers correspond to the following values: $\vartheta = \{2.5, 3 \text{ and } 4\} \mathrel{\hat{=}} \{470, 620 \text{ and } 920\,^{\circ}\text{C}\}$ $U_{\text{cell}} = \{31, 34 \text{ and } 38\} \mathrel{\hat{=}} \{796, 873 \text{ and } 976\,\text{mV}\}$.

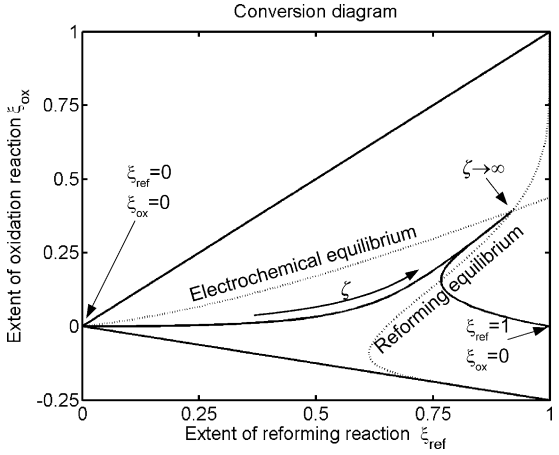

Fig. 6. Two exemplary trajectories for identical temperature and cell voltage, but with different inlet conditions. Both end up in the same attractor point, which is the intersecting point of the reforming and the oxidation equilibrium lines.

reaction rate means that the gas state moves to the right, while a positive oxidation rate causes a move upwards. Together, both reaction rates form a vector indicating in which direction the state moves along the spacial coordinate.

All reactions are considered to be reversible, so the gas composition may attain equilibrium for one or both reactions in the anode channel. In Fig. 5, several equilibrium lines are displayed for different temperatures. On these lines, the reaction rate of the corresponding reaction equals zero. The reforming equilibrium lines start from the right bottom corner and end in the right upper corner of the admissible region. How far they reach to the left only depends on the given temperature. In general, low temperatures come with a low equilibrium conversion of the reforming reaction, thus the equilibrium curve reaches far to the left. Reforming equilibrium lines can be calculated from Eq. (13) by setting the rate to zero and then solving for a function $\xi_{\text{ref}}(\xi_{\text{ox}})$, at which the reforming reaction rate is zero.

The oxidation equilibrium line always starts at the diagrams origin point and end somewhere on the right boundary line. Their course depends on the given parameters of temperature and cell voltage. The three exemplary lines in Fig. 5 are at constant temperature, but varying cell voltage. On such a line, the oxidation process comes to a halt. The oxidation equilibrium line is calculated from Eqs. (14), (15), and (17), where both electrochemical reaction rates are set to zero. The three resulting equations then contain two independent variables, which are both extents of conversion, and two unknown potential differences. This allows to solve for a function $\xi_{\text{ox}}(\xi_{\text{ref}})$, at which electrochemical equilibrium is given.

Due to their characteristic course, there is always exactly one intersection point of both curves for given temperature and voltage. At this point, both reaction rates become zero. Thus this is a stationary point. Because the reactions always run towards their equilibrium, this stationary point is an attractor.

Two exemplary trajectories are shown in Fig. 6. The boundary condition of the first simulation is that both extents of reaction are zero, meaning that the gas is neither reformed or oxidised the channel entrance. Upon entering, the reforming reaction starts and as soon as there is a significant amount of hydrogen available, the oxidation reaction rate also increases. Thus, the trajectory moves from the origin to the right and then starts to move upward as well. For an infinite channel length, the trajectory ends in the attractor point. The same holds true for a different inlet condition. Assume a completely reformed gas entering the anode channel. It ends up in the same attractor point as does the other trajectory, but on its way, the reforming reaction runs in backward direction and the reforming equilibrium line is crossed in a vertical manner.

4. Applications

The steady state anode model can be applied for numerous studies. In the following, three of them are demonstrated. They are

- a comparison of different combinations of reforming concepts,
- the simulation and numerical evaluation of the benefit of a fuel cell cascade,
- the simulation of an anode exhaust gas recycle.

4.1. Comparison of reforming concepts

As indicated in Fig. 2, three different concepts are known for reforming in high temperature fuel cell systems. The steady state anode model allows comparing the various com-

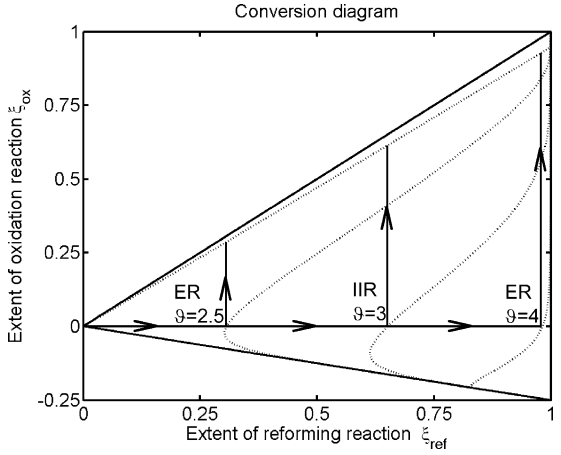

Fig. 7. Trajectories for various reforming configurations without DIR.

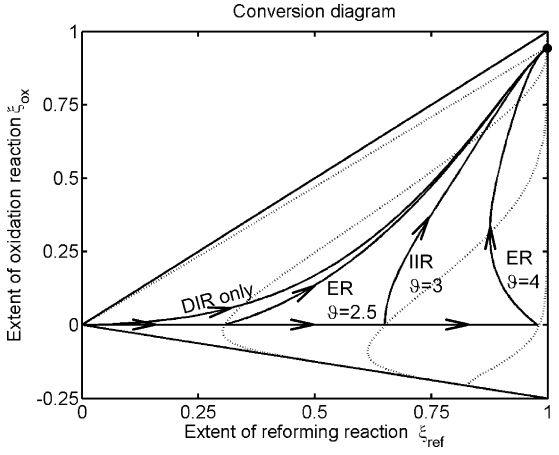

Fig. 8. Trajectories for various reforming configurations with DIR. High degrees of fuel utilisation are reachable. Compare to Fig. 7.

binations of these in an illustrative way. First, consider a system without reforming catalyst inside the anode channel, that means without DIR. Three alternatives for the fuel gas treatment are discussed:

- A low temperature ER, which can easily be heated by the hot exhaust gases of the cell.
- An IIR, where the reforming temperature is identical to the cell temperature.
- A high temperature ER, which requires additional external heating.

In this application, all three reforming units are considered to be infinitely long, thus equilibrium is reached in each unit. The exhaust gas of the reforming unit is fed into the anode channel, where only oxidation reaction takes place.

The resulting trajectories are plotted in Fig. 7. Low temperature ER and IIR produce anode fuel gas, which is reformed to an extent of 30 and 65%, respectively. The following fuel cell can only reach fuel utilisations of 25 and 60%, which is unsatisfying, because large parts of the fuel are not used. Only the high temperature ER offers the possibility to reach high fuel utilisation of about 90%, but its clear drawback is the need for extra heating, which surely would decrease the overall efficiency. Thus none of these alternatives is satisfying.

The situation changes significantly when DIR is applied. Fig. 8 shows that independent of the pre-treatment of the gas, high fuel utilisations can be reached, as all trajectories end in one single point close to the right upper corner. Here, the high temperature ER has one additional drawback: As the cell temperature is lower than the reforming temperature, the reforming reaction runs in backward direction in the first part, spoiling the high degree of reforming conversion. The same attractor point can be reached by a system without pre-treatment, where the fresh gas is directly fed into the anode channel.

This consideration clearly shows the advantage of the DIR concept. Independent of the pre-treatment of the feed gas, the application of DIR always leads to high degrees of fuel utilisation. The steady state anode model together with its conversion diagram serves as an illustrative tool here.

4.2. Anode cascade

Various authors consider appropriate flow sheets for fuel cell systems. Fellows [5] proposes to employ a cascade of fuel cells, operating at different cell voltages, to increase the overall electric power output. The proposal is that the exhaust gas of the first cells anode channel is fed into a second cell and so on. The cascade discussed here consists of two cells (Fig. 9).

Concerning electric connections, two different configurations are possible (Fig. 10). If each cell is operated not only at its own cell voltage, but it also has an independent cell current, they are connected as parallel current sources and both require a separate electrical converter (Fig. 10a). The alternative is that although their cell voltage differs, the same cell current runs through both cells (Fig. 10b). This series con-

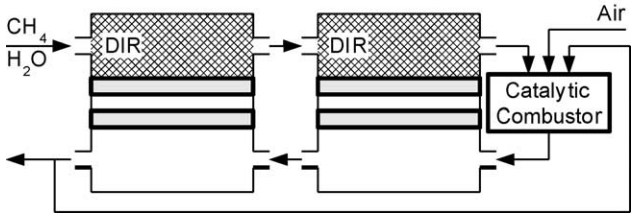

Fig. 9. Flow sheet for fuel cell cascade.

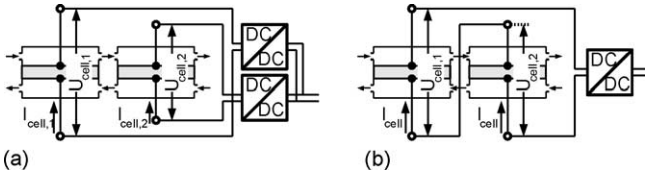

Fig. 10. Electric configurations of fuel cell cascade: (a) parallel configuration with independent cell voltage and cell current; (b) series configuration with independent cell voltage and equal cell current.

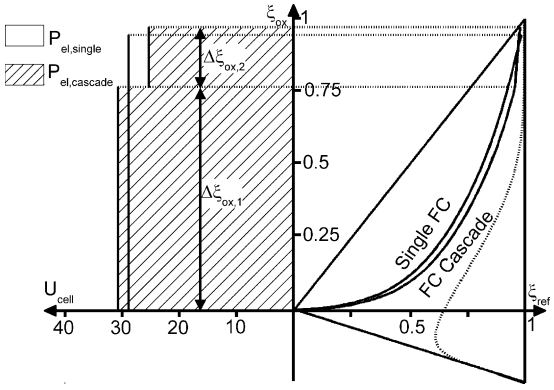

Fig. 11. Trajectories for fuel cell cascade in electric parallel configuration (for quantitative results see Table 1).

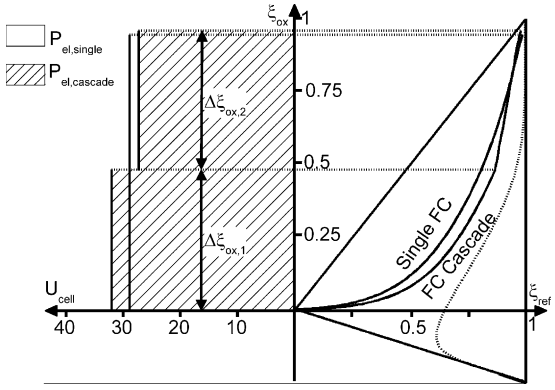

Fig. 12. Trajectories for fuel cell cascade in electric series configuration (for quantitative results see Table 1).

nection requires only one electrical converter, thus it needs less hardware effort. Both versions are discussed here.

The two cascade configurations are compared to a single cell, which has the same size as the sum of the cell sizes in each cascade. Each system is optimised to yield an optimum of electric power at a constant feed rate. The optimisation variables are the cell voltage for the single cell system, and both cell voltages plus the size of the first cell for both cascade configurations.

Fig. 11 shows the resulting trajectories for the parallel configuration in comparison to the single cell. The electric power output is illustrated by the rectangles on the left of the vertical axis. Their area is the product of the cell voltage and the advance in oxidation conversion over each cell. Table 1 shows that the electric power output of the cascade configuration exceeds that of the single cell by 4.6%.

The trajectory for the series connection is shown in Fig. 12. The differences of oxidation conversion over both cells are equal, so the additional condition of equal cell currents in both cells is fulfilled. This condition leads to a smaller increase of electric power, nevertheless an additional benefit of 3.7% due to the cascade configuration at constant feed rate can be considered relevant.

According to these calculations, the option of applying fuel cell cascades to increase the electric power output and thereby increase the system efficiency is an interesting option. From an economical point of view, the additional hardware effort necessary to build such a system stands against this configuration, at least for small systems. For large systems, where several stacks are combined in a plant, this might be profitable. The benefit of the steady state anode model in this case goes beyond illustration and intuitive understanding, but it can also serve here as a tool for a first quantitative system design and it allows conducting first economical calculations.

Table 1
Optimisation results of single cell and both two-cell cascades

	Length ζ	Voltage U_{cell}	Extent of oxidation reaction $\Delta\xi_{ox}$	El. power P_{el}
Single	1.0	28.83	0.947	62.40
Parallel cascade				
1. Cell	0.674	30.81	0.683	48.10
2. Cell	0.326	27.00	0.278	17.17
Total	1.0	–	0.961	65.27 (+4.6%)
Series cascade				
1. Cell	0.508	31.84	0.480	34.93
2. Cell	0.492	27.20	0.480	29.84
Total	1.0	–	0.960	64.70 (+3.7%)

4.3. Anode exhaust gas recycling

In literature one can also find the proposal to recycle a part of the anode exhaust gas back towards the inlet [5,6] (Fig. 3). Especially for pure DIR systems this has certain advantages: if fresh feed gas is fed into the anode channel, no hydrogen is present at the inlet and thus the electrode is unused in this region. This can be amended by recycling part of the exhaust gas, which still contains some hydrogen, back to the inlet.

Define the recycle flow via a recycle ratio according to:

$$R = \frac{\tilde{\Gamma}_{\text{feed}}}{\tilde{\Gamma}_{\text{back}}} \tag{20}$$

Then the mixing rules (Eqs. (9) and (10)) simplify to

$$\tilde{\Gamma}_{\text{in}} = (1 + R)\,\tilde{\Gamma}_{\text{feed}} \tag{21}$$

$$\xi_{j,\text{in}} = \frac{\xi_{j,0} + R\xi_{j,\text{back}}}{1 + R} \tag{22}$$

Fig. 13 shows the trajectory of a single cell without ($R = 0$) and with anode gas recycling ($R = 0.3$). Both are operated at individual optimal cell voltage, so that electric power is maximised. While the inlet condition of the system without recycle is at the origin, the inlet condition of the recycle system is calculated via the law of the lever (Eq. (19)) from the conditions of the feed gas and the anode exhaust gas.

The electric power output of the system with gas recycle is always lower than what one gets from the system without recycling. This can be explained in two ways, both of them have the same basis. The first explanation is that back mixing always worsens the reactor performance in systems with a positive order of reaction. Thus the higher the recycling ratio gets, the lower the electric power output becomes.

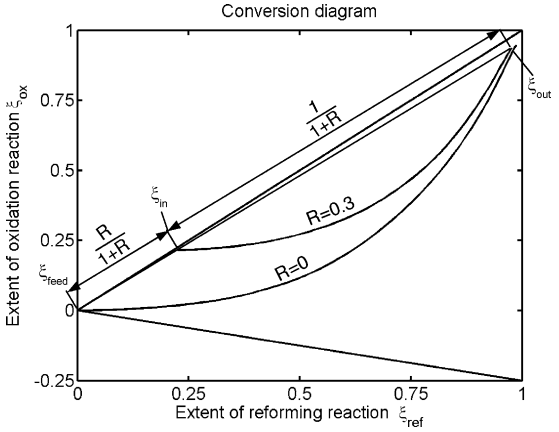

Fig. 13. Trajectories for systems without and with anode gas recycling.

The other explanation uses the conversion diagram (Fig. 13). For DIR systems with unreformed feed, the trajectories are usually bent to the left hand side. This means that the inlet condition of a recycle system, which lies on a straight line between inlet and outlet condition, can only lie within the bent of the corresponding no-recycle system. This means that the trajectory lies closer to the main diagonal. In this region, lower cell voltages must be applied in order to achieve comparable oxidation rates and therefore reach high fuel utilisations. Consequently, the electric power output of the cell is decreased due to the necessity to apply lower cell voltage.

Although this result speaks against the application of the anode gas recycling, it does not consider the temperature effects of such a measure. There might be benefits that compensate for the loss in power output. For example, feeding fresh gas into a DIR-channel leads to high reforming reaction rates at the inlet. Consequently, the temperature drops sharply, leading to strong temperature gradients. These have to be avoided, and the recycling of anode exhaust gas is expected to homogenise the temperature profile. This application shows another potential use of the model, but it also hints at one of its limitations, that are the neglect of a temperature distribution.

5. Conclusions

The steady state anode model is a simple and easily understandable tool for the analysis of various aspects of the interaction of reforming and oxidation reaction in high temperature fuel cells. It is small, mathematically simple, fast to solve, flexible and can easily be interpreted by physical means. The phase diagram of the model, the conversion diagram, is a useful and intuitive tool for the display and interpretation of the simulation results. Although the model is applied to MCFC here, it can easily be adapted to fit for SOFC as well. The basic phenomena shown here are the same for both fuel cell types.

All three applications which are shown here yield qualitative results, one of them gives quantitative results suitable for system design. The first of them, the comparison of different reforming concepts, is an illustrative pleading in favour of the DIR concept, the direct internal reforming in the anode channel. The benefit of fuel cell cascades compared to single cells is estimated in the second application, proving its usefulness for conceptual system design. Results indicate that considerable power increase can be expected, but the additional hardware effort might spoil the benefit for smaller systems. The third application demonstrates that gas recycling spoils the system performance. This application also reveals the limitations of the steady state anode model, as temperature effects are not considered. Further applications of the model and its accompanying diagram are possible.

Acknowledgement

The authors gratefully acknowledge the funding of the research project “Optimierte Prozessführung von Brennstoffzellensystemen mit Methoden der Nichtlinearen Dynamik” by the German Federal Ministry of Education and Research (BMBF) under the Grant 03C0345 A.

Appendix A

A.1. Derivation of the steady state anode model

The partial and the total mass balance for the anode channels in molar terms under the given model assumptions read [7,8]:

$$\gamma \frac{\mathrm{d}\chi_i}{\mathrm{d}\zeta} = \sum_{j=\mathrm{ref,ox}} (\nu_{i,j} - \chi_i \bar{\nu}_j) \mathrm{Da}_j r_j \tag{A.1}$$

$$\frac{\mathrm{d}\gamma}{\mathrm{d}\zeta} = \sum_{j=\mathrm{ref,ox}} \bar{\nu}_j \mathrm{Da}_j r_j \tag{A.2}$$

with

$$\chi_i(\zeta = 0) = \chi_{i,\mathrm{in}} \tag{A.3}$$

$$\gamma(\zeta = 0) = \Gamma_{\mathrm{in}} \tag{A.4}$$

Expressing the molar fraction via reaction extents (Eq. (7)), these equations transform to:

$$\frac{\mathrm{d}\xi_j}{\mathrm{d}\zeta} = \frac{\mathrm{Da}_j r_j}{\gamma \xi_{j,\max}} \left(1 + \sum_{j=\mathrm{ref,ox}} \bar{\nu}_j \xi_j \xi_{j,\max} \right) \tag{A.5}$$

$$\frac{\mathrm{d}\gamma}{\mathrm{d}\zeta} = \gamma \times \frac{\sum_{j=\mathrm{ref,ox}} \bar{\nu}_j (\mathrm{d}\xi_j/\mathrm{d}\zeta) \xi_{j,\max}}{1 + \sum_{j=\mathrm{ref,ox}} \bar{\nu}_j \xi_j \xi_{j,\max}} = \gamma \times \frac{f'(\zeta)}{f(\zeta)} \tag{A.6}$$

with the boundary conditions

$$\xi_j(\zeta = 0) = \xi_{j,\mathrm{in}} \tag{A.7}$$

$$\gamma(\zeta = 0) = \Gamma_{\mathrm{in}} \tag{A.8}$$

The solution of Eq. (A.6) and its boundary condition in Eq. (A.8) is

$$\gamma = \tilde{\Gamma}_{\text{in}} \times \left(1 + \sum_{j=\text{ref,ox}} \bar{\nu}_j \xi_j \xi_{j,\max}\right) \tag{A.9}$$

Inserting this into Eq. (A.5), we receive the desired ODE describing the progress of the extents of reaction along the channel:

$$\frac{\mathrm{d}\xi_j}{\mathrm{d}\zeta} = \frac{\mathrm{Da}_j r_j}{\tilde{\Gamma}_{\text{in}}} \times \frac{1}{\xi_{j,\max}} \tag{A.10}$$

A.2. Reaction kinetics

The reaction kinetics is described using potential kinetics combined with Arrhenius terms for the temperature influence and Butler-Volmer kinetics for the electrochemical reactions. The molar fractions in the following reaction rate expressions are calculated from the extents of reaction according to Eq. (7). The reforming reaction rate reads:

$$r_{\text{ref}} = \exp\left(\mathrm{Arr}_{\text{ref}}\left(\frac{1}{\vartheta^0_{\text{ref}}} - \frac{1}{\vartheta}\right)\right) \times \left\{\chi_{\text{CH}_4}\chi^2_{\text{H}_2\text{O}} - \frac{\chi_{\text{CO}_2}\chi^4_{\text{H}_2}}{K_{\text{eq,ref}}(\vartheta)}\right\} \tag{A.11}$$

The electrochemical oxidation rate reads:

$$r_{\text{ox}} = \exp\left(\mathrm{Arr}_{\text{ox}}\left(\frac{1}{\vartheta^0_{\text{ox}}} - \frac{1}{\vartheta}\right)\right) \times \exp\left(\frac{\Delta\phi_{\text{a}} - \Delta\phi_{\text{ox},0}(\vartheta)}{\vartheta}\right) \times \left\{\chi_{\text{H}_2} - \chi_{\text{H}_2\text{O}}\chi_{\text{CO}_2} \times \exp\left(-2\frac{\Delta\phi_{\text{a}} - \Delta\phi_{\text{ox},0}(\vartheta)}{\vartheta}\right)\right\} \tag{A.12}$$

The electrochemical reduction rate corresponds to the description of the superoxide mechanism from Prins-Jansen [9]:

$$r_{\text{red}} = \exp\left(\mathrm{Arr}_{\text{red}}\left(\frac{1}{\vartheta^0_{\text{red}}} - \frac{1}{\vartheta}\right)\right) \times \exp\left(2.5\frac{\Delta\phi_{\text{c}} - \Delta\phi_{\text{red},0}(\vartheta)}{\vartheta}\right) \times \left\{\chi^{-2}_{\text{CO}_2,\text{c}} - \chi^{0.75}_{\text{O}_2,\text{c}}\chi^{-0.5}_{\text{CO}_2,\text{c}} \times \exp\left(-3\frac{\Delta\phi_{\text{c}} - \Delta\phi_{\text{red},0}(\vartheta)}{\vartheta}\right)\right\} \tag{A.13}$$

Note that the overpotentials of both reactions can be found in the argument of the exponential function, as is shown here for the anodic reaction:

$$\eta_{\text{a}} = \Delta\phi_{\text{a}} - \Delta\phi_{\text{ox},0}(\vartheta) \tag{A.14}$$

Here, the Nernst voltage at standard gas composition occurs as a temperature dependent function, $\Delta\phi_{\text{ox},0}(\vartheta)$.

A.3. Cathode gas composition

The cathode gas composition corresponds to the exhaust gas of a complete combustion of the feed gas with a specific amount of air. The air amount is determined via an air number according to:

$$\Gamma_{\text{air}} = \frac{\lambda_{\text{air}}}{\chi_{\text{O}_2,\text{air}}} \times \Gamma_{\text{feed}} 2\chi_{\text{CH}_4,\text{feed}} \tag{A.15}$$

The total mass balance of the combustion yields the cathode outlet flow:

$$\Gamma_{\text{c}} = \Gamma_{\text{feed}} + \Gamma_{\text{air}} \tag{A.16}$$

The partial mass balances deliver the molar fractions of the cathode gas as:

$$\chi_{\text{CO}_2,\text{c}} = \frac{\Gamma_{\text{feed}}\chi_{\text{CH}_4,\text{feed}}}{\Gamma_{\text{c}}} \tag{A.17}$$

$$\chi_{\text{H}_2\text{O},\text{c}} = \frac{\Gamma_{\text{feed}}(\chi_{\text{H}_2\text{O},\text{feed}} + 2\chi_{\text{CH}_4,\text{feed}})}{\Gamma_{\text{c}}} \tag{A.18}$$

$$\chi_{\text{O}_2,\text{c}} = \frac{\Gamma_{\text{air}}\chi_{\text{O}_2,\text{air}} - \Gamma_{\text{feed}}2\chi_{\text{CH}_4,\text{feed}}}{\Gamma_{\text{c}}} \tag{A.19}$$

$$\chi_{\text{N}_2,\text{c}} = \frac{\Gamma_{\text{air}}\chi_{\text{N}_2,\text{air}}}{\Gamma_{\text{c}}} \tag{A.20}$$

There are no further components present in the cathode gas.

A.4. Used model parameter values

All variables are dimensionless.

	Da_j	Arr_j	Equilibrium	Feed	Air/Others
Reforming	25	84.4	$K_{\text{eq,ref}} = \exp\left(26.22 - \frac{75.83}{\vartheta}\right)$	S/C = 2.5	$\lambda_{\text{air}} = 2.2$
Oxidation	5	21.6	$\Delta\phi_{\text{ox},0} = 28.26 - 19.84\vartheta$	$\Gamma_{\text{feed}} = 1$	$\chi_{\text{O}_2,\text{air}} = 0.21$
Reduction	0.3	31.2	$\Delta\phi_{\text{red},0} = 78.00 - 23.06\vartheta$		$F = (1 + \text{S/C})/8$

References

[1] W. He, Q. Chen, J. Power Sources 73 (1998) 182–192.
[2] F. Yoshiba, et al., J. Power Sources 71 (1998) 328–336.
[3] M.D. Lukas, K.Y. Lee, H. Ghezel-Ayagh, Control Eng. Practice 10 (2002) 197–206.
[4] H.-K. Park, et al., J. Power Sources 104 (2002) 140–147.
[5] R. Fellows, J. Power Sources 71 (1998) 281–287.
[6] P.J. Kortbeek, R. Ottervanger, J. Power Sources 71 (1998) 223–225.
[7] P. Heidebrecht, K. Sundmacher, Chem. Eng. Sci. 58 (2003) 1029–1036.
[8] P. Heidebrecht, K. Sundmacher, Fuel Cells 3–4 (2002) 166–180.
[9] J.A. Prins-Jansen, K. Hemmes, J.H.W. de Wit, Electrochim. Acta 42 (1997) 3585–3600.